# Multibody Dynamic Modeling and Control of an Unmanned Aerial Vehicle under Non-Holonomic Constraints

Eric Lanteigne and Joshua O'Reilly

***Abstract*—This paper presents the application of the Boltzmann-Hamel equations to the modeling of a multibody lighter-than-air vehicle. The vehicle is composed of a lifting gas envelope and movable gondola for performing rapid descent maneuvers. The vehicle pitch is primarily controlled by the position of the gondola on the keel of the envelope. The pitch control law was treated as a non-holonomic constraint applied to the system dynamics. The derivation of the equations of motion are presented for a simplified case, and the effectiveness and performance are demonstrated through numerical simulations using theoretical and experimental aerodynamic model parameters.**

## I. Introduction

Unmanned aerial vehicles (UAV) are complex aeronautical systems that are rapidly replacing manned aircraft missions and creating new opportunities where air-, space- and ground-based sensors cannot reach. In recent years, commercialization of fixed-wing and rotor-based unmanned aircraft has gained significant traction as governments develop regulatory frameworks and industry invests in new markets. For these reasons, the challenges associated with the dynamics, control, planning, task allocation, and detection of UAVs, amongst others, have received much attention. While model-free techniques such as reinforcement learning have been applied to the control of flight-tested non-linear aerial vehicles [1], the development of a dynamic model remains a valuable tool in the creation and verification of the controller and autopilot behavior.

In classical mechanics, the two fundamental methods for developing dynamic models of mechanical systems are the Lagrangian and Newton-Euler mechanics. The former involves kinetic and potential energies whereas the later involves the combination of translational and rotational dynamics using Euler's laws of rigid body motion about the center of gravity. As an example, the procedure to obtained the dynamic equations for a quad-rotor vehicle using either methods is demonstrated in [2] and the results are identical.

The dynamic equations of aerial and underwater vehicles have traditionally been developed using the Newton-Euler mechanics [3], [4]. The resulting six degree-of-freedom model is typically expressed as the sum of the lumped inertia matrix, centrifugal and Coriolis matrix, damping matrix, and gravitational and buoyancy vectors. These models have been studies extensively in recent years owing a resurgence in lighter-than-air (LTA) vehicle interest and, as a consequence, numerous control strategies for this model have been explored [5]–[8]. These models are relatively simple to construct under the assumption that the center of gravity remains constant [9], or the vehicle remains neutrally buoyant [10], or for vehicles with few degrees of freedom. For higher order systems, such as aircraft with retractable landing gear or where rotor dynamics are taken into account, multibody dynamic equations have been constructed using the Jourdain principle of virtual power [11].

Authors are with the Department of Mechanical Engineering at the University of Ottawa, Ottawa, Canada



The renewed interest in LTAs is fueled by two main potential application gaps: heavy lift transport to remote locations, and high endurance aerial monitoring. With respect to the latter, a reconfigurable unmanned airship comprised of a helium envelope with a moving gondola at its keel was modeled and simulated [12]. The key attribute of this vehicle is the ability to perform rapid descent manoeuvres, an important consideration for recovering unmanned LTAs. The dynamic model was based on the typical Euler-Lagrange formulation and neglected the gondola dynamics. As a consequence, large oscillatory motions were observed during flight tests [13]. To improve the flight dynamics, a multi-body dynamic model using the Boltzmann-Hamel equations was developed using quasi-velocities of the vehicle, where quasi-velocities are defined as being relative to a configuration-dependent reference frame. Furthermore, a control law guiding the gondola motion was incorporated into the model as a non-holonomic constraint superimposed on the equations of motion of the vehicle [14]. Non-holonomic constraints are non-integrable constraints on the motion and/or non-integrable quasi-velocities which, when using the classical form of Lagrange's equations, require the inclusion of Lagrange multipliers to account for reaction forces of the non-holonomic constraints [15], [16]. The Boltzmann-Hamel equations can be applied to dynamic systems with non-holonomic constraints and/or quasi-velocities directly. When control strategies are formulated as non-holonomic constraints on the quasi-velocities, it is possible to integrate tracking directly in the dynamic model.

This paper provides details on the derivation of the individual terms of the Boltzmann-Hamel equation for the reconfigurable airship and the gondola position controller. The vehicle model was restricted to planar motions to facilitated and simplify the presentation of the method. The remainder of this paper is organised as follows. First, the dynamic model of the airship using the Boltzmann-Hamel equations is developed.

The simulation setup and results are then presented. Finally, conclusions are reached as to the effectiveness of the proposed method.

## II. Dynamic Model

### A. Kinematics

A schematic of the multi-body reconfigurable blimp is shown in Figure 1. It is composed of a helium envelope of mass $m_1 = m_{envelope} + m_{rail} + m_{helium}$ and a movable gondola of mass $m_2$ which supports the longitudinal and lateral thrusters, the gondola position controller, the autopilot, and the batteries. The body reference frame is fixed to the center of volume (CV) which is assumed to be coincident with the envelope center of gravity ($\mathrm{CG_e}$) located at $m_1$.

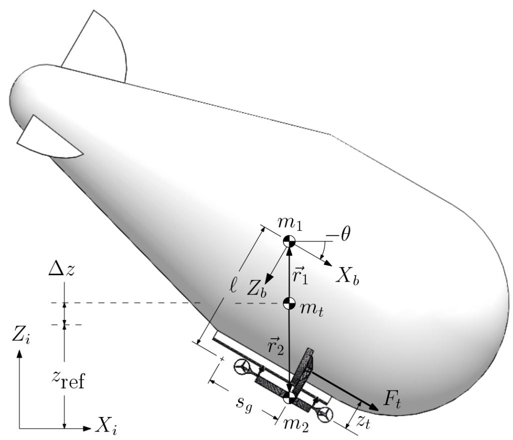


Fig. 1. Reconfigurable blimp model and coordinate system

To simplify the development and presentation of the multi-body dynamic model, the lateral motion, yaw and roll rotations are neglected, reducing to a two dimensional system. The generalized coordinates expressed in the inertial reference frame $[X_i \; Z_i]$ as

$$\vec{q} = \begin{bmatrix} x & z & \theta & s_g \end{bmatrix} \tag{1}$$

where $x$ is the displacement along $X_i$, $z$ is the displacement along $Z_i$, $\theta$ is the pitch (with $\theta = 0^{\text{o}}$ indicating level flight), and $s_g$ is the gondola displacement along the rail. The gondola position $s_g = 0$ m indicates that the gondola $\mathrm{CG_g}$ intersects the vertical axis $Z_b$ of the CV. Airships are typically modelled in the body reference frame $[X_b \;\; Z_b]$ fixed to the CV, as the aerodynamic forces generated by the lifting gas envelope are significant and modelled about this point. Since airships operate at a specific neutrally buoyant altitude $z_{\text{ref}}$, the altitude of the vehicle $\mathrm{CG_v}$, located at the total mass of the vehicle $m_v = m_1 + m_2$, can further be defined as $z = \Delta z + z_{\text{ref}}$.

The coordinates of the helium envelope and gondola with respect to the vehicle CG in the inertial reference frame are obtained by solving the following two vector equations:

$$\vec{r}_1 + \ell \begin{bmatrix} \sin\theta \\ -\cos\theta \end{bmatrix} + s_g \begin{bmatrix} \cos\theta \\ \sin\theta \end{bmatrix} = \vec{r}_2 \tag{2}$$

$$m_1 \vec{r}_1 + m_2 \vec{r}_2 = 0 \tag{3}$$

where $\vec{r_1}$ is the vector from the vehicle $\mathrm{CG_v}$ to the envelope $\mathrm{CG_e}$, $\vec{r_2}$ is the vector from the vehicle $\mathrm{CG_v}$ to the gondola $\mathrm{CG_g}$, and $\ell$ is the distance from the envelope $\mathrm{CG_e}$ to the gondola $\mathrm{CG_g}$ along $Z_b$. From (2) and (3), the following relations can be obtained:

$$\begin{bmatrix} r_{1x} \\ r_{2x} \end{bmatrix} = \begin{bmatrix} -k_2(\ell\sin\theta + s_g\cos\theta) \\ k_1(\ell\sin\theta + s_g\cos\theta) \end{bmatrix} \tag{4}$$

$$\begin{bmatrix} r_{1z} \\ r_{2z} \end{bmatrix} = \begin{bmatrix} k_2(\ell\cos\theta - s_g\sin\theta) \\ -k_1(\ell\cos\theta - s_g\sin\theta) \end{bmatrix} \tag{5}$$

where $k_2 = m_2/m_v$ and $k_1 = m_1/m_v$.

### B. Kinetic Energy

The kinetic energy of the envelope can be expressed in three parts: the contribution of the relative motion between $m_1$ and the vehicle $\mathrm{CG_v}$, the contribution of the velocity with respect to the inertial reference frame, and the rotational kinetic energy:

$$T_1 = \frac{1}{2} m_1 \dot{\vec{r}}_1^T \dot{\vec{r}}_1 + \frac{1}{2} m_1 \dot{\vec{r}}^T \dot{\vec{r}} + \frac{1}{2} J_1 \dot{\theta}^2 \tag{6}$$

where $J_1 = J_{envelope} + J_{rail} + J_{helium}$ are the moments of inertia of the main components of the helium envelope, and $\vec{r}$ is the vector from the origin to the vehicle CG in the inertial reference frame. In the longitudinal plane, the gondola is treated as a point mass with $m_2$ and its kinetic energy is simply expressed as

$$T_2 = \frac{1}{2} m_2 \dot{\vec{r}}_2^T \dot{\vec{r}}_2 + \frac{1}{2} m_2 \dot{\vec{r}}^T \dot{\vec{r}} \tag{7}$$

The total kinetic energy $T(\dot{\vec{q}}, \vec{q}, t)$, expressed in the generalized coordinates, is then given by

$$T = T_1 + T_2 = \frac{1}{2} \dot{\vec{q}}^T \begin{bmatrix} m_v I_2 & 0_2 \\ 0_2 & B_{\text{CG}} \end{bmatrix} \dot{\vec{q}} \tag{8}$$

where $I_2$ is the $2 \times 2$ identity matrix and

$$B_{\text{CG}} = \begin{bmatrix} J_1 + k_1 m_2(\ell^2 + s_g^2) & k_1 m_2 \ell \\ k_1 m_2 \ell & k_1 m_2 \end{bmatrix} \tag{9}$$

is symmetric and positive definite matrix of the kinetic energy of the vehicle relative to its $\mathrm{CG_v}$ [17].

### C. Potential Energy

The potential energy of the vehicle less the potential energy of the displaced air is given by

$$U = g\big((m_1 - m_{\text{air}})(z + r_{1z}) + m_2(z + r_{2z})\big) \tag{10}$$

The intended maximum operating altitude of the blimp is 122 m (400 ft) as per the Canadian Aviation Regulations on small remotely piloted systems [18]. For low altitude flights and for the purpose of evaluating the model, the following assumptions were made:

1) The envelop is rigid with a constant volume $V_1$.

2) The atmospheric temperature is 20°C.
3) The change in air density was approximated by $\Delta\rho = -1.31\mathrm{e}^{-4}\mathrm{kg/m}^4$.

For a given altitude $z$, $\rho_{\text{air}}$ can be approximated by

$$\rho_{\text{air}} = \rho_{\text{ref}} - \Delta\rho\Delta z \tag{11}$$

where $\rho_{\text{ref}}$ is the air density at $z_{\text{ref}}$. At this reference altitude, $m_{\text{air}} = \rho_{\text{ref}}V_1 = m_v$ and the following expression describes the relation between $m_{\text{air}}$ and $m_v$:

$$m_{\text{air}} = \frac{\rho_{\text{ref}} - \Delta\rho\Delta z}{\rho_{\text{ref}} - \Delta\rho z_{\text{ref}}} m_v \tag{12}$$

## III. Boltzmann-Hamel Differential Dynamic Model

The direct application of the Lagrangian approach does not produce correct equations of motion if the kinetic energy is expressed in terms of quasi-velocities rather than true velocities [19]. This is typically the case for UAVs, where the angular velocities are expressed in the body reference frame.

### A. Quasi-Velocities

In an unconstrained system such as single-body UAVs, the relation between quasi-velocities and the derivatives of the generalized coordinates is of the form

$$u_j = \sum_{i=1}^{n} \Psi_{ji}(q,t)\dot{q}_i + \Psi_{jt}(q,t) \quad j = 1,\ldots,n \tag{13}$$

where $n$ is the number of degrees of freedom of the system [16]. Furthermore, with $\Psi_{ji} = \Phi_{ij}^{-1}$ and $\Psi_{jt} = \Phi_{it}$, the following inverse relation can be obtained:

$$\dot{q}_i = \sum_{j=1}^{m} \Phi_{ij}(q,t)u_j + \Phi(q,t)_{ij} \tag{14}$$

For a system with $m$ non-linear time-dependent rheonomic constraints, the last $m$ quasi-velocities are chosen such that constraints result in $u_j = 0$. This can be expresses as

$$\begin{gathered} u_j = \sum_{i=1}^{n} \Psi_{ji}(q,t)\dot{q}_i + \Psi_{jt}(q,t) = 0 \\ j = n-m+1,\ldots,n \end{gathered} \tag{15}$$

For the airship shown in Figure 1, the quasi-velocities $u_{1-3}$ in the longitudinal plane are the velocities in the body-reference frame. These are given by

$$u_1 = \dot{x}\cos\theta + \dot{z}\sin\theta \tag{16}$$

$$u_2 = -\dot{x}\sin\theta + \dot{z}\cos\theta \tag{17}$$

$$u_3 = \dot{\theta} \tag{18}$$

The airship pitch $\theta$ has show strong dependence on the gondola position $s_g$ whereas the longitudinal velocity $u_1$ is mainly affected by the thrust $F_t$ [20]. Moreover, research presented in [14] has shown that the controller of an unmanned aircraft can be formulated using constraints on the quasi-velocities. Therefore, pitch $q_3$ was linked to the gondola position $q_4$ in the form of a non-holonomic constraint on the system. For the present vehicle, a PI controller was selected for the gondola position.

$$s_g = k_p(\theta - \theta_d) + k_i \int (\theta - \theta_d)dt \tag{19}$$

The forth quasi-velocity $u_4$ can then be obtained by taking the time derivative of (19) and converting the result into a non-linear constraint.

$$u_4 = k_p\dot{\theta} - \dot{s}_g + (-k_p\dot{\theta}_d + k_i\theta - k_i\theta_d) = 0 \tag{20}$$

This results in the following coefficient matrices:

$$\Psi_{ji}(q,t) = \begin{bmatrix} \cos q_3 & \sin q_3 & 0 & 0 \\ \sin q_3 & -\cos q_3 & 0 & 0 \\ 0 & 0 & 1 & 0 \\ 0 & 0 & k_p & -1 \end{bmatrix} \tag{21}$$

$$\Psi_{jt}(q,t) = \begin{bmatrix} 0 \\ 0 \\ 0 \\ -k_p\dot{\theta}_d + k_i\theta - k_i\theta_d \end{bmatrix} \tag{22}$$

The generalized form of the Boltzmann-Hamel equation representing the minimum number $n-m$ of first-order dynamic equations for a system with rheonomic constraints is given by

$$\begin{gathered} \frac{d}{dt}(\frac{\partial L}{\partial u_r}) - \sum_{i=1}^{n} \frac{\partial L}{\partial q_i}\Phi_{ir} + \sum_{j=1}^{n}\sum_{l=1}^{n-m} \frac{\partial L}{\partial u_j}\gamma_{rl}^j u_l \\ + \sum_{j=1}^{n} \frac{\partial L}{\partial u_j}\gamma_r^j = F_r \qquad r = 1,\ldots,n-m \end{gathered} \tag{23}$$

where $n$ is the configuration space and $m$ is the number of non-holonomic constraints.The Hamel coefficients $\gamma_{rl}^j$ and $\gamma_r^j$ associated with rheonomic constraints are defined as

$$\gamma_{rl}^j(q,t) = \sum_{i=1}^{n}\sum_{k=1}^{n} \left(\frac{\partial\Psi_{ji}}{\partial q_k} - \frac{\partial\Psi_{jk}}{\partial q_i}\right)\Phi_{kl}\Phi_{ir} \tag{24}$$

$$\begin{gathered} \gamma_r^j(q,t) = \sum_{i=1}^{n}\sum_{k=1}^{n} \left(\frac{\partial\Psi_{ji}}{\partial q_k} - \frac{\partial\Psi_{jk}}{\partial q_i}\right)\Phi_{kt}\Phi_{ir} \\ + \sum_{i=1}^{n} \left(\frac{\partial\Psi_{ji}}{\partial t} - \frac{\partial\Psi_{jt}}{\partial q_i}\right)\Phi_{ir} \end{gathered} \tag{25}$$

While the Boltzmann-Hamel equation and quasi-velocities were presented for rheonomic constraints, the gondola controller (19) is a scleronomic constraint since the controller gains $k_{i,p}$ are time-invariant. Therefore, the time derivatives $\partial\Psi_{ji}/\partial t$ in $\gamma_r^j$ are all equal to zero. The remainder of the terms in (24) and (25) are simply the derivatives of (21) and (22) with respect to each generalized coordinate.

The Lagrangian is composed of the unconstrained kinetic and potential energies expressed in terms of the quasi-velocities $L(\vec{u},\vec{q},t)$. Therefore, the kinetic energy (8) must be converted to quasi-coordinates. It is also important to note that all $n$ partial derivatives of the Lagrangian with respect to the quasi-velocities $\partial L/\partial u_j$ in (23) must be computed before the last $m$ quasi-velocities are set to zero ($u_4 = 0$ in the case of the present example). Similarly, $\vec{F}$, the vector of applied forces and torques, is expressed in terms of quasi velocities. If the external forces are formulated according to the generalized coordinates, the individual terms $F_r$ can be obtained with the following transformation:

$$F_r = \sum_{i=1}^{n} Q_i \Phi_{ir} \tag{26}$$

where $Q_i$ is the applied force or torque associated with the generalized coordinate $q_i$, expressed in terms of generalised coordinates $\vec{q}$. For aircraft in general, the applied forces and torques are typically functions of the propeller thrust and the aerodynamic lift and drag. Since these forces are generally already described in terms of quasi velocities, they can be applied to (23) directly. The unmanned airship described in this paper has two forward-facing thrusters located on the port and starboard sides at $z_t$ above the gondola center of gravity. In the longitudinal plane, the thrust generated by each propeller $F_p$ is assumed to be equal. The total thrust $F_t = 2F_p$ produces the following vector of applied forces and torques about the vehicle CG:

$$\vec{T} = F_t \begin{bmatrix} 1 & 0 & \ell(1-k_2) - z_t & 0 \end{bmatrix}^T \tag{27}$$

The aerodynamic forces and torques of airships are typically described in the body reference frame $[X_b \; Z_b]$ fixed to the CV, as the helium envelop area is significantly larger than the gondola. Since the dynamic model is defined about the vehicle $\mathrm{CG_v}$, the longitudinal and vertical forces contribute to the aerodynamic moment according to

$$\vec{A} = \begin{bmatrix} 1 & 0 & 0 \\ 0 & 1 & 0 \\ -k_2\ell & -k_2 s_g & 1 \end{bmatrix} \begin{bmatrix} A_{x_b} \\ A_{z_b} \\ A_\theta \end{bmatrix}. \tag{28}$$

where $A_{x_b,z_b,\theta}$ are the aerodynamic forces about the CV. In the body reference frame, these forces are dependent on the angle of attack, the dynamic pressure and the drag coefficients [4]. A comprehensive method for obtaining the aerodynamic properties for small LTA vehicles is described in [21]. The applied forces and torques vector described in terms of quasi-velocities is then obtained from $\vec{F} = \vec{T} - [\vec{A}^T \; 0]^T$.

## IV. Simulation and Results

Pitch trajectory tracking was performed to evaluate the effectiveness of treating the gondola position controller as a nonlinear constraint on the dynamic model. The flowchart of the simulation is shown in Figure 2.

The airship physical parameters used in the simulator are based on measurements of the prototype vehicle when available or estimated from literature; these are listed in Table I. The mass and inertia of the rail was assumed to be negligible compared to the helium envelop and was neglected

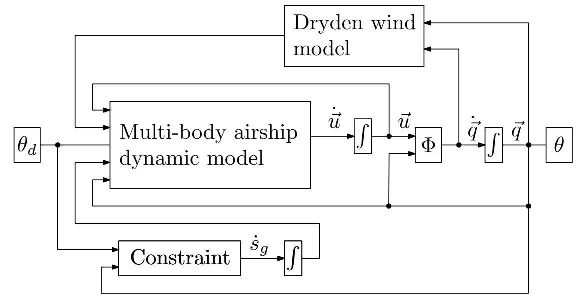


Fig. 2. Guidance control loop flowchart

TABLE I
Airship parameters

| | | | | | |
|---|---|---|---|---|---|
| $m_1$ | 2.2 kg | $m_2$ | 5.4 kg | $J_1$ | 2.73 kgm$^2$ |
| $\ell$ | 1.11 m | $z_t$ | 0.27 m | $z_{\text{ref}}$ | 180 m |

in the simulations. The gondola is equipped with two forward-facing 11 inch propellers. According to previous works, the motor/propeller combination was capable of producing a combined maximum static thrust of 5.2 N and a combined maximum dynamic thrust of 3.2 N at a forward velocity of 4 m/s [22]. Tracking data was recorded for 200 s at a constant thrust input. For the purpose of demonstrating the controller, the motor and propeller dynamics and velocity induced thrust reduction were neglected. This assumption was deemed reasonable since in most cases the vehicle reached its steady state velocity in under 10 s. Simulations were performed for three thrust levels from $F_t$ = 1 to 3 N, resulting in approximate average velocities of 2.0, 3.5, and 4.0 m/s respectively. Moreover, the gondola speed $\dot{s}_g$ was limited to 0.1 m/s as this is the maximum speed measured on the prototype airship.

The model and controller were simulated for $0 < k_p < 1$ and $0 < k_i < 2$ values for sinusoidal and step reference pitch trajectories of $\pm 30°$ and 100 s periods, and average wind speeds of 0.35 and 0.70 m/s. Figure 3 illustrates the general effects of the controller gains on the root mean square error of the tracking for a step reference pitch trajectory. Higher values of $k_i$ and lower values $k_p$ provide stable tracking performance.

The tracking results are presented for the more aggressive case of $F_t$ = 3 N with an average lateral wind speed of 0.7 m/s in Figures 4 to 7. The airship exhibits a tracking error of approximately 1.8$^\circ$ for a 30$^\circ$ sinusoidal reference pitch trajectory and 0.5$^\circ$ for a 30$^\circ$ step reference pitch trajectory once the tracking angle is reached. The differences between the minimum and maximum values of $s_g$ in the step reference trajectory is mainly attributed to the constant positive torque produced by the thrusters $T(3)$ in (27). This torque is negated by maintaining a slightly forward gondola position. In addition to the thruster-generated torque, the vehicle was subjected to random vertical wind component which, during the 50 to 100 s time period, was substantially lower than the average wind speed of 0 m/s specified in the Dryden model. The vertical and angular wind components are shown in Figure 8. This further reduced the rearward gondola position required to maintain a

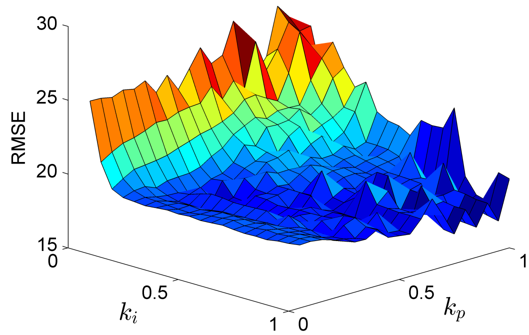


Fig. 3. Root mean square error of the pitch tracking for a step reference pitch trajectory with $F_t$= 3 N and $V_{\text{wind}}$ = 0.35 m/s. Similar trends were observed at lower thrust levels and higher wind speeds.

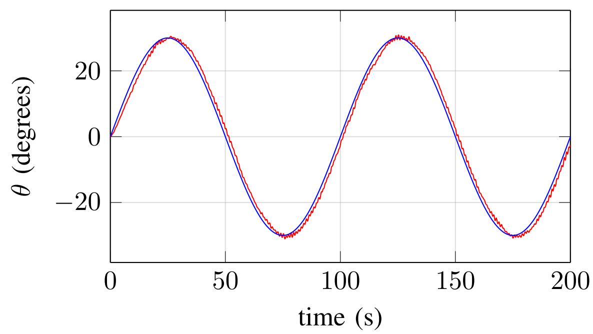


Fig. 4. Vehicle pitch angle (red) and reference pitch angle (blue) for sine control signal

positive 20º pitch angle.

The oscillatory behaviour of the gondola velocity $\dot{s}_g$ observed in Figure 9 is a consequence of the low theoretical aerodynamic damping moment computed using the methodology developed for larger airships [21], [23]. Preliminary tests on the prototype airship indicate a larger aerodynamic damping moment, therefore variations in $\dot{s}_g$ are expected to be lower. An experimental evaluation of the aerodynamic terms will be conducted using the methodology similar to that presented in [24] once the prototype is completed.

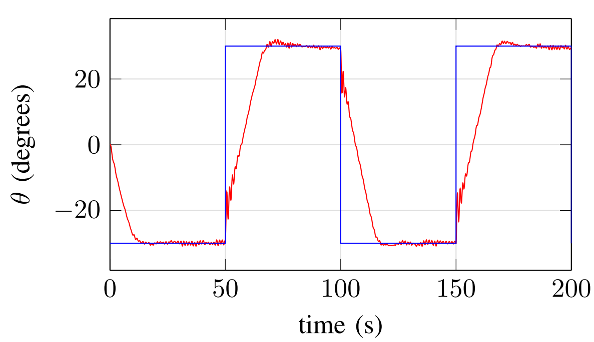


Fig. 5. Vehicle pitch angle (red) and reference pitch angle (blue) for square control signal

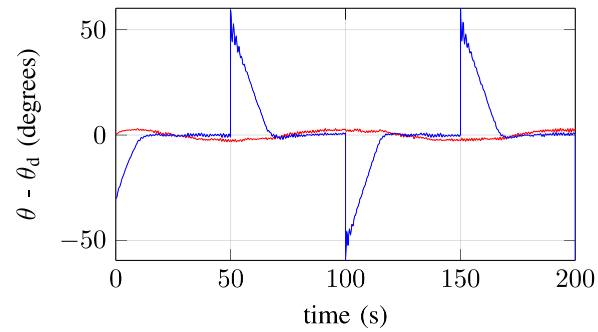


Fig. 6. Tracking error for sine (red) and square (blue) control signals

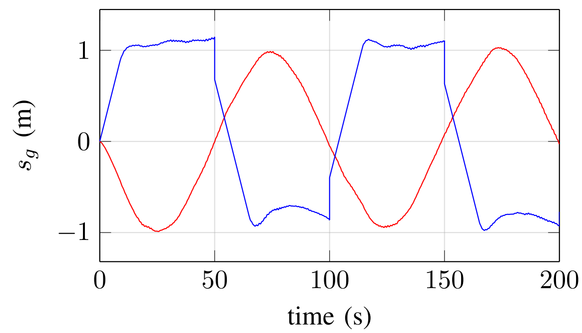


Fig. 7. Gondola position $s_g$ for sine (red) and square (blue) control signals

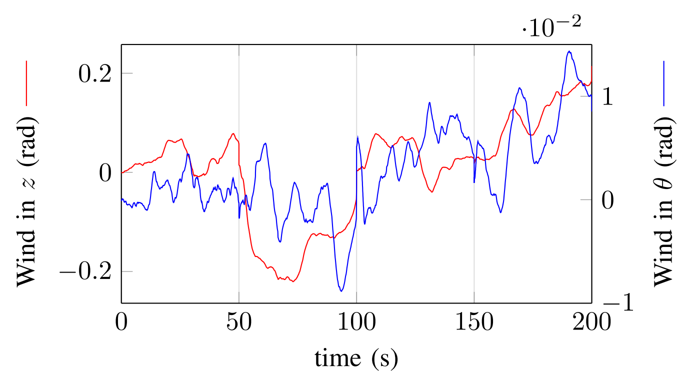


Fig. 8. Vertical and angular wind components

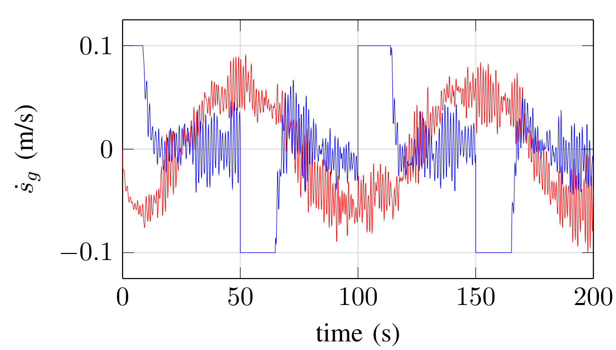


Fig. 9. Gondola velocity $\dot{s}_g$ for sine (red) and square (blue) control signals

## V. Conclusions

This paper describes the development of the dynamic model of a multibody unmanned aerial vehicle using the Boltzmann-Hamel equations with a guidance law formulated as a non-holonomic constraint. The simulation results demonstrate that the vehicle is capable of tracking multiple trajectories with low error under a wide range of gain parameters. While only a simplified version of the model is presented, the methodology described in this paper can easily be applied to the full dynamic model of the airship or any other multi-body aerial vehicle. Moreover, the guidance laws can be formulated to account for additional bodies and non-holonomic constraints.

## References


[1] M. Abouheaf and W. Gueaieb, "Online model-free controller for flexible wing aircraft: a policy iteration-based reinforcement learning approach," *International Journal of Intelligent Robotics and Applications*, Oct 2019.

[2] L. R. G. Carrillo, A. E. D. López, R. Lozano, and C. Pégard, *Quad Rotorcraft Control: Vision-Based Hovering and Navigation*, ser. Advances in Industrial Control. London: Springer-Verlag, 2013.

[3] T. I. Fossen, *Guidance and Control of Ocean Vehicles*. Wiley, 1994.

[4] B. L. Stevens, F. L. Lewis, and E. N. Johnson, *Aircraft Control and Simulation: Dynamics, Controls Design, and Autonomous Systems*. Wiley-Blackwell, Oct. 2015.

[5] L. Sangjong, H. Lee, W. Daeyeon, and B. Hyochoong, "Backstepping Approach of Trajectory Tracking Control for the Mid-Altitude Unmanned Airship," in *AIAA Guidance, Navigation and Control Conference and Exhibit*. South Carolina: American Institute of Aeronautics and Astronautics, Aug. 2007.

[6] Y.-N. Yang, J. Wu, and W. Zheng, "Trajectory tracking for an autonomous airship using fuzzy adaptive sliding mode control," *Journal of Zhejiang University SCIENCE C*, vol. 13, no. 7, pp. 534–543, Jul. 2012.

[7] K. Y. Pettersen and O. Egeland, "Position and Attitude Control of an Underactuated Autonomous Underwater Vehicle," in *In Proceeding of the IEEE Conference on Decision and Control. IEEE*, 1996, pp. 987–991.

[8] T. Elmokadem, M. Zribi, and K. Youcef-Toumi, "Control for Dynamic Positioning and Way-point Tracking of Underactuated Autonomous Underwater Vehicles Using Sliding Mode Control," *Journal of Intelligent & Robotic Systems*, vol. 95, no. 3, pp. 1113–1132, Sep. 2019.

[9] M. E. Nørgaard Sørensen, S. Hansen, M. Breivik, and M. Blanke, "Performance Comparison of Controllers with Fault-Dependent Control Allocation for UAVs," *Journal of Intelligent & Robotic Systems*, vol. 87, no. 1, pp. 187–207, Jul. 2017.

[10] Y. Yang, J. Wu, and W. Zheng, "Positioning Control for an Autonomous Airship," *Journal of Aircraft*, vol. 53, no. 6, pp. 1638–1646, 2016.

[11] R. Leitner and P. Koppitz, "Quick Modeling of Fixed- and Rotary-Wing Aircrafts using a synthetic tree structured Multibody Approach," in *AIAA Modeling and Simulation Technologies Conference*, 2012, pp. 1–12.

[12] E. Lanteigne, A. Alsayed, D. Robillard, and S. G. Recoskie, "Modeling and control of an unmanned airship with sliding ballast," *Journal of Intelligent & Robotic Systems*, vol. 88, no. 2, pp. 285–297, Dec 2017.

[13] A. Alsayed and E. Lanteigne, "Experimental pitch control of an unmanned airship with sliding ballast," in *International Conference on Unmanned Aircraft Systems*, 2017, pp. 1640–1646.

[14] E. Ładyżyńska Kozdraś, "Modeling and numerical simulation of unmanned aircraft vehicle restricted by non-holonomic constraints," *Journal of Theoretical and Applied Mechanics*, vol. 50, no. 1, pp. 251–268, 2012.

[15] J. M. Cameron and W. J. Book, "Modeling Mechanisms with Nonholonomic Joints Using the Boltzmann-Hamel Equations," *The International Journal of Robotics Research*, vol. 16, no. 1, pp. 47–59, 1997.

[16] J. I. Neimark and N. A. Fufaev, *Dynamics of Nonholonomic Systems*. Amer. Mathem. Society, 1972.

[17] F. Aghili, "Modeling and Control of Mechanical Systems in Terms of Quasi-Velocities," in *Robotics 2010: Current and Future Challenges*. InTech, 2010.

[18] G. of Canada, "901.25 (1)," Nov 2019.

[19] D. T. Greenwood, *Advanced Dynamics*. Cambridge University Press, 2003.

[20] A. Mansur and E. Lanteigne, "Pitch tracking for an airship with moving gondola using backstepping control," in *International Conference on Mechatronics and Robotics Engineering*, 2020.

[21] S. G. Recoskie, "Autonomous hybrid powered long ranged airship for surveillance and guidance," Ph.D. dissertation, University of Ottawa, 2014.

[22] D. Muzar, E. Lanteigne, and J. McLeod, "Dynamic characterization of brushless dc motors and propellers for flight applications," *Unmanned Systems*, vol. 5, no. 3, pp. 159–167, 2017.

[23] J. B. Mueller, M. A. Paluszekt, and Y. Zhao, "Development of an aerodynamic model and control law design for a high altitude airship," in *Collection of Technical Papers - AIAA 3rd "Unmanned-Unlimited" Technical Conference, Workshop, and Exhibit*, vol. 1, 2004, pp. 415–431.

[24] C. Blouin, "Trajectory optimization of a small airship," Master's thesis, University of Ottawa, 2015.